JOURNAL OF OPTOELECTRONICS AND ADVANCED MATERIALS Vol. 10, No. 4, April 2008, p. 737 - 743

*Invited Paper*

# Half-metallic ferromagnetism and spin polarization in $CrO_2$: a detailed VCA study

H. ALLMAIER[a,*], L. CHIONCEL[a,b], E. ARRIGONI[a], E. BURZO[c], F. BEIUSEANU[b], M. I. KATSNELSON[d], A. I. LICHTENSTEIN[e]

[a] *Institute of Theoretical Physics, Graz University of Technology, A-8010 Graz, Austria*
[b] *Department of Physics, University of Oradea, RO-410087 Oradea, Romania*
[c] *Faculty of Physics, Babes-Bolyai university RO-400084 Cluj-Napoca, Romania*
[d] *Institute for Molecules and Materials, Radboud University of Nijmegen, NL-6525 ED Nijmegen, The Netherlands*
[e] *Institute of Theoretical Physics, University of Hamburg, 20355 Hamburg, Germany*

We present a combined electronic structure and many-body calculation for the half-metallic ferromagnet $CrO_2$. A realistic three-band Hubbard Hamiltonian is used to describe the relevant $t_{2g}$ orbitals which is solved within a self consistent variational cluster approach. To demonstrate the robustness of our results we show that results does not change significantly when increasing the dimension of clusters.

(Received February 25, 2008; accepted April 2, 2008)

*Keywords*: Half metallic ferromagnet, Band structure, Magnetic properties, $CrO_2$, Three-band Hubbard hamiltanian

## 1. Introduction

Transition metal oxides exhibit a rich collection of interesting and intriguing properties, which can be used for a wide variety of applications including quantum computing using Cooper pairs, ultra high-density magnetic data storage and more recently spintronic applications [1]. Among these materials $CrO_2$ is an outstanding example in which magnetism and correlation effects associated with electron-electron interaction determine the essential finite temperature properties such as polarization and magnetisation [2]. New effects resulting as interplay of various phenomena attracted an increasing attention to motivate the investigation of the electronic properties of $CrO_2$ by a multitude of experimental [3-9] and theoretical approaches [10-13]. Despite the large number of investigations, the understanding of the correlated electronic structure of $CrO_2$ is still not complete.

$CrO_2$ is besides the full and semi-Heuslers, the most prominent half-metallic ferromagnetic compound [14]. Its half-metallic character was predicted by Schwarz [15], and its high spin polarization of more than 90% was found in point contact measurements at superconductor metal interfaces [16, 17]. Consequently it is an interesting candidate for spintronics. This very large spin polarization taken at *1.6 K*, is still far from being ideal 100%. Even at low temperatures, magnons can be excited, which can suppress the ideal spin polarization. We have shown for a large number of half-metals in the semi-Heusler and zinc-blende structure that a qualitative description of the electron-magnon interaction captured by the Dynamical-Mean Field Theory (DMFT), leads to the existence of non-quasiparticle states (NQP) [2,18-21]. These states produce a drastic depolarization, their effect being dominant in comparison with other effects such as spin-orbit interaction or non-collinearity [19]. Obviously in the complicated realistic structure of the half-metallic ferromagnets, effects like imperfections spin disorder or phonons may play a role in depolarization. Nevertheless in perfect crystals, the NQP states should play an important role.

In this article we analyze in detail how the many-body electron-electron interaction affects the spin down density of states, in particular how the NQP states are generated, and their consequences on the polarization of $CrO_2$. In a previous paper [2] we discussed the spin-polarization of $CrO_2$ using a self-consistent cluster perturbation theory, namely the variational cluster approach (VCA) [22-25] that includes also non-local correlation effects of special importance. Here we extend our previous work [2] by comparing several results with the existing experimental studies. We describe the form of the interacting Hamiltonian for both model and realistic electronic structure calculations and present results of the spectral function, density of states and finite scaling. Finally, the paper is summarized with the conclusions of our results.

## 2. Interacting Hamiltonian

$CrO_2$ is an oxide ferromagnet with the Curie temperatures of 385-400 K [26]. The electrical resistivity has a metallic temperature dependence and shows anomalies around $T_c$ indicating scattering of electrons by fluctuating magnetic moments at finite temperatures. At low temperatures, optical spectroscopy at 10 K [4] demonstrates a saturation magnetization of 1.92 $\mu_B$ which is close to the ideal value of 2 $\mu_B$.

$CrO_2$ shows a rutile structure with Cr-ions forming a tetragonal body-centered lattice. $Cr^{4+}$ has a closed shell Argon core and in addition two *3d*-electrons. The Cr-ions are sitting in the center of $CrO_6$-octahedra and thus experience crystal field splitting. Therefore, the 3d-orbitals are split into a $t_{2g}$-triplet and an excited $e_g$-doublet. The cubic symmetry is further reduced to tetragonal due to a

distortion of the octahedra, which partially lifts the degeneracy of the $t_{2g}$-orbitals into a $d_{xy}$ ground-state and $d_{yz-zx}$ and $d_{yz+zx}$ excited states. With only two 3d-electrons we can neglect the energetically higher lying $e_g$-states and focus solely on the $t_{2g}$-triplet. In the following subsections we discuss the Hamiltonian which describes only the $t_{2g}$-orbitals using model and realistic parameters for the electron-electron Coulomb interaction.

In the followings we introduce the multi-orbital Hamiltonian relevant for the $t_{2g}$-orbitals. In the most general form this can be written as:

$$H = H_0 + \frac{1}{2}\sum_{i,m,\sigma} U_{mm'm''m'''} c^+_{im\sigma} c^+_{im'\sigma'} c_{im'''\sigma'} c_{im''\sigma} \quad (1)$$

where $c^+_{im\sigma}$ and $c_{im\sigma}$ are the usual fermionic creation and annihilation operators operating on an electron with spin $\sigma$ at site $i$ in the $t_{2g}$-orbital $m$ (either being $d_{xy}$, $d_{yz}$ or $d_{zx}$). $H_0$ is the non-interacting part obtained by the downfolding procedure using the $N$-th order muffin-tin orbital (NMTO) method using the local-density approximation (LDA) [27,28]. Using this method we effectively include also the $e_g$-orbitals, which are left out in the VCA calculation, since they renormalize the $t_{2g}$ hopping and on-site energy parameters of the $t_{2g}$-orbitals. The hopping and the interacting part can be written in the form:

$$\begin{aligned} H &= \sum_{i,m,\sigma} t_{im\sigma,jm'\sigma} c^+_{im\sigma} c_{im'\sigma'} \\ H_I &= \frac{1}{2}\sum_{i,m,\sigma} U_{mmmm} n_{im\sigma} n_{im-\sigma} \\ &+ \frac{1}{2}\sum_{i,m\neq m'} (U_{mm'mm'} - \tfrac{1}{2} J_{mm'mm'}) n_{im} n_{im'} \\ &- \sum_{i,m\neq m'} S_{im} S_{im'} \end{aligned} \quad (2)$$

$t_{im\,\sigma,\,jm'\sigma} = (\varepsilon_m, t_{im\sigma,\,jm'\sigma})$ denotes both the on-site energies $\varepsilon_m$ and the hopping from a site and orbital $(i,m)$ to the site and orbital $(j,m')$. We included the chemical potential $\mu$ in the the expression for the on-site energies $\varepsilon_m$. In general a further simplification is taken namely that in the full scalar product $\mathbf{S}_{im}\mathbf{S}_{im'}$ only the $z$-component is kept, so that the interacting Hamiltonian takes the usual form of $U$, $U'$ and $U'$-$J$. In our calculation we keep the full scalar product and rewrite the Hamiltonian by decoupling the $S_zS_z$ and $S_+S_-$ components:

$$\begin{aligned} H_I &= \frac{1}{2}U\sum_{i,m,\sigma} n_{im\sigma} n_{im-\sigma} \\ &+ \frac{1}{2}U\sum_{i,m\neq m'} n_{im\sigma} n_{im'-\sigma} \\ &+ \frac{1}{2}(U'-J)\sum_{i,m\neq m'} n_{im\sigma} n_{im'\sigma} \\ &+ J\sum_{i,m\neq m'} c^+_{im\uparrow} c^+_{im'\downarrow} c_{im\downarrow} c_{im'\uparrow} \\ &+ J\sum_{i,m,\sigma} c^+_{im\uparrow} c^+_{im'\downarrow} c_{im\uparrow} c_{im'\downarrow} \end{aligned} \quad (3)$$

The on-site Coulomb interaction takes the following form: the usual term $U_{mmmm}=U$, the off-diagonal direct coupling term $U_{mm'mm'}=U'$ and the exchange coupling $U_{mm'mm'}=J$ [29]. Since above stated Hamiltonian includes spin- and pair-flip terms as well, spin-rotational invariance is conserved. The pair-hopping term is also included via $U_{mmm'm'}=J$. The Coulomb-interaction $U$ and Hund's exchange $J$ parameters between $t_{2g}$ electrons are evaluated from first principles by means of a constrained LSDA method [30]. While this method is not very accurate, and may produce slightly different values depending on its exact implementation, it is quite clear that for $CrO_2$ the interaction parameters are not too strong.

For a realistic description of the Coulomb interactions, the non-zero matrix elements $U_{mm'm''m'''}$ can be computed for the particular material taken into account the symmetry of the orbitals and crystal structure. It is important to remember that the energy $U$ of Coulomb interaction is rather large - 15-30eV - in free atoms consisting of *3d* transition metals. In solids the screening is very efficient and leads to much smaller values of $U$ [31]. In the present work we compared the results for the model Hamiltonian description, where the approximate values *U~3eV* and *J~0.9eV* are used with the realistic multiplet calculation of the Coulomb interaction, presented below.

The Coulomb and exchange interaction energy of a pair of interacting electrons situated in a particular $d$ orbital $m$ and $m'$ is calculated from the Slater integrals $F^k$ [30]: $U_{mm'mm'}=\Sigma_k\ a_k\ F^k$ and $J_{mm'mm'}=\Sigma_k\ b_k\ F^k$, with the coefficients $a_k$ and $b_k$ given in terms of integrals over the products of spherical harmonics [30]:

$$\begin{aligned} a_k &= \tfrac{4\pi}{2k+1}\sum_{q=-k}^{k} \langle lm|Y_{kq}|lm\rangle\langle lm'|Y^*_{kq}|lm'\rangle \\ b_k &= \tfrac{4\pi}{2k+1}\sum_{q=-k}^{k} |\langle lm|Y_{kq}|lm'\rangle|^2 \end{aligned} \quad (4)$$

The sum over all $k>0$ results in non-zero *3j* symbols. The *3j*-symbols vanish for odd $k$ and $k_{max}=2l$ for $d$ electrons. The non-vanishing matrix elements of the Coulomb interaction are grouped into direct and exchange interactions: $U=U_{mmmm}$, $U'=U_{mm'mm'}$ and $J=U_{mm'mm'}$. Within the real harmonics basis for the $t_{2g}$ orbitals, they have the expression:

$$\begin{aligned} U &= F_0 + 4F_2 + 36F_4 \\ U' &= F_0 - 2F_2 - 4F_4 \\ J &= 3F_2 + 20F_4 \end{aligned} \quad (5)$$

The above results for the non-zero matrix elements in the basis of real spherical harmonics differs from the equations previously reported [1,32]. It can be seen that the condition $U'=U-2J$ is fulfilled and no additional conditions are required as claimed in [1,32]. The presence of spin-flip and pair-flip terms in the expression of the Hamiltonian makes the Hamiltonian spin-rotational invariant, while the orbital rotational invariance is broken by the presence of different orbitally selective hoppings $t_{mm'}$, due to the realistic crystal structure.

## 3. Variational Cluster Approach (VCA)

VCA accesses the physics of a lattice model in the thermodynamic limit by optimizing trial self-energies generated by a reference system. The reference system consists of an isolated cluster having the same interaction as the original lattice, but differing in the single-particle part of the Hamiltonian. An approximation to the self-energy of the lattice model is then obtained by finding the saddle point of an appropriate grand-canonical potential

$$\Omega = \Omega' + Tr.\ln G_{VCA} - Tr.\ln G_{cl} \qquad (6)$$

with respect to the single-particle parameters of the reference system [23]. Here, $G_{cl}$ is the Green's function matrix of the reference system (cluster), which is calculated numerically as a function of frequency and spin. The lattice Green's function $G_{VCA}$ is obtained by a matrix form of the Dyson equation, whereby the self-energy $\Sigma$ of the reference system is used as an approximation to the lattice self-energy. $\Omega$ and $\Omega'$ are the grand-canonical potential of the lattice, respective the reference system.

To solve the reference system, that is the "cluster" part of the VCA procedure an exact diagonalization (Lanczos) technique is used. For the multi-orbital Hamiltonian presented in the previous sections memory requirements are considerable, therefore calculations were performed for clusters consisting of up to eight sites. We stress that hoppings not included within the clusters are not neglected, but taken into account in the noninteracting lattice Green's function entering the Dyson equation in the expression for the VCA Green's function.

Quite generally, multi-orbital strongly-correlated systems show a competition between different magnetic

and orbital-ordered phases. In order to check that the ferromagnetic phase is the one with the lowest energy, we have compared its grand-canonical potential with the one of different magnetic phases containing mixed antiferromagnetic and ferromagnetic components in different directions. Notice that the particle density in the physical system is in general different from the one of the reference system [25]; the former turns out to be slightly doped with $n=1.83$ particles per unit cell (for eight sites). Moreover, for the chosen parameters we confirm that the ferromagnetic state is more favorable energetically with respect to all antiferromagnetic states we have considered, as well as to the paramagnetic state.

Corrections for a ``double-counting" of the interaction only produces an irrelevant constant shift of the chemical potential [33], as we are considering a model Hamiltonian with fixed number of electrons.

## 4. Results

Results of the VCA calculations are presented for the density of states and the spectral functions. We discuss how these results change when increasing the dimension of the cluster (reference system), and how they compare with the Dynamical Mean Field Theory results.

### 4.1. Density of states

A remarkable result of the VCA calculation is the presence of a significant amount of states at the Fermi energy originating from the putatively localized $d_{xy}$ orbital. More specifically, we obtain that this orbital is not completely half filled, its occupation being $n^{xy}\sim 0.87$, while for the other two orbitals we have $n^{yz+zx}\sim 0.49$, and $n^{yz-zx}\sim 0.45$. This is also confirmed by LSDA+DMFT calculations [2]. Consequently, the $d_{xy}$ orbital consists of quite itinerant electrons, though with a large effective mass rather than of localized moments. Notice that our findings are in contrast to previous DMFT [34,35] calculations, in which the Fermi energy only touches the high-energy tail of the $d_{xy}$ DOS, which can then be considered as localized moments. This is probably due to the large value of the interaction parameter $U$ used in these calculations. We believe that the smaller value of $U\sim 3eV$ used here is more appropriate, as it is obtained from first principles.

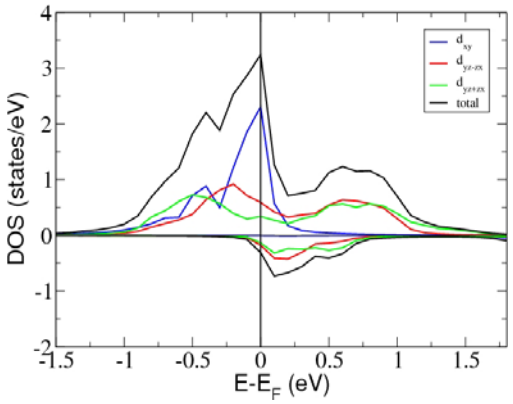


*Fig. 1. Cr-$t_{2g}$ orbital-resolved density of states in the ferromagnetic state, calculated within the LDA+VCA approach for U = 3 eV, and J = 0.9 eV, using an 8 site cluster.*

In the minority spin channel, NQP states are clearly visible predominantly in the $d_{yz\pm zx}$ orbitals just above the Fermi energy. The physical origin of NQP states is connected with the ``spin-polaron" processes [36,37]: the spin-down low-energy electron excitations, which are forbidden for half-metallic ferromagnets in the one-particle picture, turn out to be possible as superpositions of spin-up electron excitations and virtual magnons [36,37]. An uniform superposition forms a state with the same total spin quantum number $S=(N+1)/2$ ($N$ is the particle number in the ground state) as the low-energy spin-up state, but with one ``spin-flip", i. e. with $z$-component $S_z$=S-1. If the Hamiltonian is spin-rotation invariant this state with one additional spin-down particle must have the same energy as the low-energy state with one additional spin-up particle, although its weight is reduced by a factor $1/N$. We stress that spin-rotation invariance is crucial in order to obtain low-energy NQP states. For this reason, methods neglecting spin flip processes in eq.1 are not expected to provide a correct description of NQP states. Similar NQP

states are obtained in the fully self-consistent LSDA+DMFT calculation [2].

### 4.2. Spectral function

The VCA method allows to investigate many-body physical effects due to the *k*-dependence of the self-energy of the cluster. *k*-dependent many-body effects are very important and were observed in the photoemission experiments of cuprate superconductors. Within the VCA approach the single-particle excitation spectrum, the so-called spectral function was calculated as: $A(k,\omega)=-(1/\pi)\,\mathrm{Im}G_{VCA}(k,z)$ with $z=\omega+i\eta$, where $\eta$ broadens the delta peak to give it a finite width.

In the case of $CrO_2$, many-body effects are responsible for the existence on NQP states. These states are situated in the minority spin channel just above the Fermi-energy ($E_F$) and their spectral function is visible in Fig.2, lower panel.

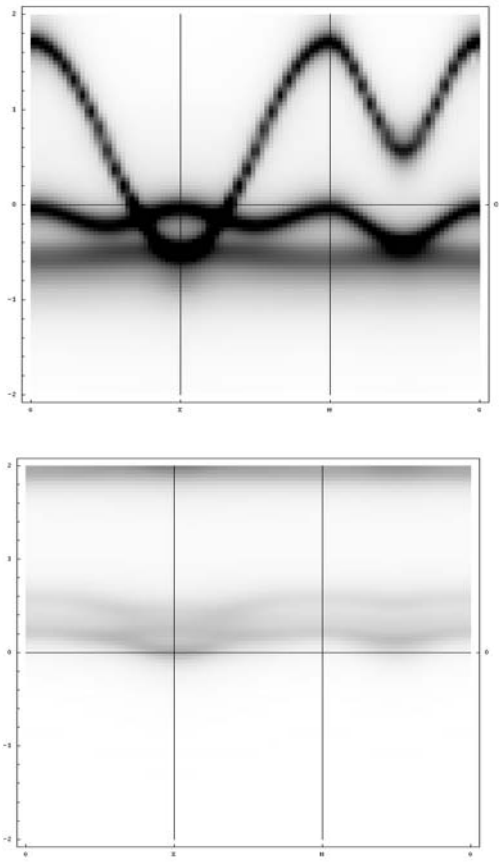

*Fig. 2. Calculated spectral function for U=3 eV, and J=0.9 eV, using an eight site cluster: top majority spin, bottom minority spin channel*

As can be seen the many-body effects are most significant at wave vectors away from Γ point. For this reason, spin-polarized photoemission at normal emission or spin-polarized inverse photoemission at normal incidence may not observe this effect. Therefore angle-resolved spin-polarized photoemission with a proper wave vector sampling is required to evidence the existence of NQP states experimentally.

In Fig.2, upper panel, it can be seen that the majority (spin-up) $d_{xy}$ band is situated close to the Fermi-energy and has a bandwidth of around 1eV. This band touches the Fermi-surface at three symmetry points, Γ,X and M, which demonstrates its itinerant rather than localized character as was considered in the previous calculations [11,38]. Around the X point the $d_{yz\pm\ zx}$ bands cross the Fermi-energy leading to the observed metallic character of the majority spin channel. A rough estimation of the bandwidth of $d_{yz\pm zx}$ orbital gives the value of around *2eV*. In the minority channel the NQP bands having a $d_{yz\pm zx}$ character only touch the Fermi-energy at the point X.

### 4.2. Finite size scalling

The quality of the gathered results depends on the choice of the reference systems and therefore we investigate finite size effects by choosing four, six and eight sites as our reference system.

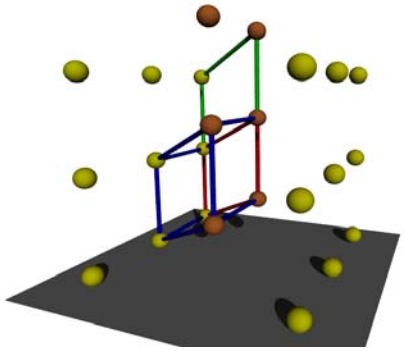

*Fig. 3. The tetragonal $CrO_2$-lattice showing the various cluster geometries: yellow and orange denote the two different Cr-sites; thered lines denote the four sites cluster (located in the (110)-plane), extended by the green lines for six sites and doubled to eight sites by the blue lines.*

Since the oxygen octahedra around the Chromium-sites on the face of the tetragonal are rotated against those located at the *bcc*-sites, all chromium-sites are no longer equivalent [28]; therefore all reference systems include the two different Chromium sites, $Cr_1$ and $Cr_2$.

Fig. 3 shows the tetragonal $CrO_2$-lattice, where the two nonequivalent chromium-sites are denoted in different colors. Different cluster geometries were considered, which individually include different hopping processes within the cluster. Since the VCA approach becomes exact in the limit of an infinitely large reference system we expect a convergence of the results when enlarging the cluster size; this is also what can be seen in the Fig. 4, where we show the DOS for each cluster size.

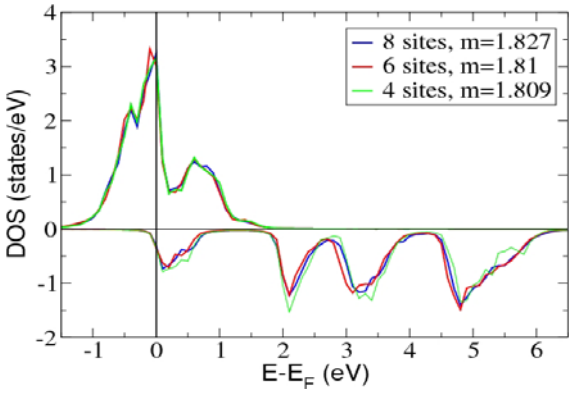


*Fig. 4. Scaling: Density of states for 4, 6 and 8 sites clusters show remarkable similarities. m denotes the calculated magnetization.*

The differences are not changing the results significantly. The most notable differences for the various cluster sizes can be seen in the minority spin channel, where the smallest cluster with four sites overestimates the peaks at *0.3 eV* and at *2 eV*, giving however the correct position. This is not the case for the peak at *3.3 eV*, where the position is shifted by roughly *0.15 eV* relative to the larger cluster sizes. Further the shape changes as well from a double peak structure of equal height to a major peak with a shoulder (as in the eight sites case). The structure further away from the Fermi-energy, around *5 eV*, is again slightly shifted; by about *0.1 eV* and also the shape itself is again affected: the small pseudo gap structure at *5.5 eV* is no longer seen in the results from the larger cluster sizes.

Since the six sites cluster is not included in the eight sites geometry, one expects to find also differences related to the inclusion of different lattice sites, which is indeed the case. Comparing the four sites result with the result from eight sites they appear to bear closer resemblance than six to either four or eight sites; most notably the minority peak at *3.3 eV* deviates in position and shape significantly from the other results. The same is true but to a lesser amount for the majority peak touching the Fermi-energy where the position of the peak is slightly changed in relation to the other results.

### 4.3. Comparison with DMFT results

In Fig. 5 we compare our results to quite recent experimental data including bremsstrahlung isochromat spectroscopy (BIS), ultraviolet photoemission (UPS) experiments done by Tsujioka et al [3] and *O1s* x-ray absorption measurements done by Huang et al [5]. The BIS-data show a rather good agreement with our minority spin results, however showing only a little shoulder at *1.75 eV* where we find a gap. This is most probably due to the onset of the oxygen-states *O1s*-states as shown in the figure. Further differences away from Fermi-energy also arise due to the fact that we do not consider in the calculations explicitly the $e_g$-states, which are located at roughly around *4 eV*.

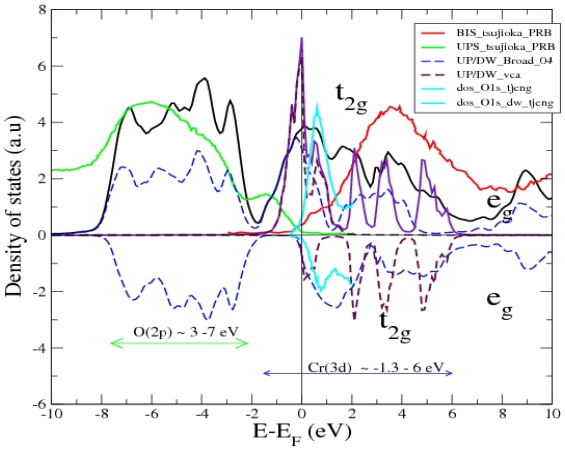


*Fig. 5. Comparison with experimental results including BIS and UPS experiments [3] and O 1s x-ray absorption measurements by Huang et al [5].*

Fig. 6 shows LSDA and DMFT-results for comparison. Notably, the LSDA Fermi level intersects the majority-spin bands near a local minimum and lies in the band gap of the minority spin states. Finite temperatures and correlation effects close this minimum around the Fermi level, as can be seen from the LDA+DMFT results in Fig.5. For both spin channels, the DOS is shifted uniformly to lower energies in the energy range of -2 and -6eV, where predominantly the *O(p)* bands are situated. This is due to the fact that correlated *Cr(d)* bands affect the *O(p)* states through the *Cr(d)-O(p)* hybridisation, so that the latter contribute actively to the mechanism of the ferromagnetic ground state. The LSDA+DMFT calculation confirms the existence of minority spin states just above the Fermi energy, as observed in the VCA calculation.

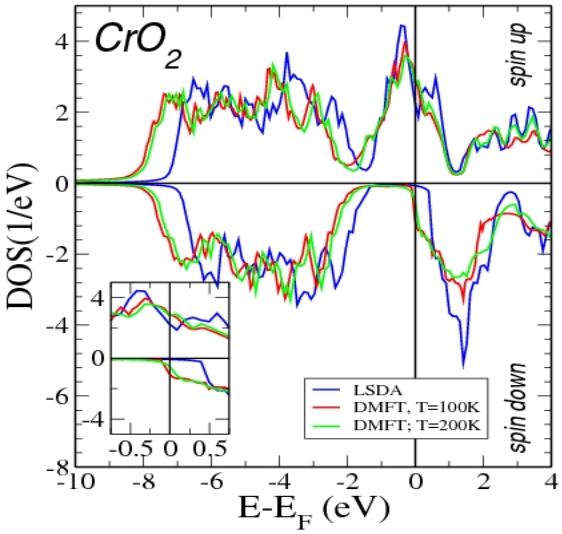


*Fig. 6. Comparison of LSDA and LSDA+DMFT results for different temperatures. The LSDA density of states is considered as the zero temperature result [2].*

Further we will show that many-body effects discussed above, especially the formation of NQP states, contribute significantly to the energy dependence of the spin polarization

$$P(E) = \frac{N_{\uparrow}(E) - N_{\downarrow}(E)}{N_{\uparrow}(E) + N_{\downarrow}(E)} \qquad (7)$$

where *N(E)* is the density of states of majority ↑ or minority ↓ electrons.

Fig. 7 shows a comparison between the measured [5] and computed polarization for the different ab-initio many-body calculations discussed in the present paper. Due to the tails of NQP states, polarization is less than *100%* even at the Fermi level. The LDA calculation clearly overestimates the spin polarization as it neglects correlation effects. On the other hand, both VCA and DMFT results show excellent agreement with the experiment at the Fermi level. At energy of about *0.5 eV* polarization is reduced by about *50%*, and up to this energy the agreement of the VCA calculation is excellent, while DMFT results overestimate depolarisation effects away from the Fermi energy.

The disagreement for energies above ~ *0.5 eV* is probably due to terms not included in the VCA Hamiltonian, eq. 1, such as $e_g$ orbitals which start becoming important at higher energies.

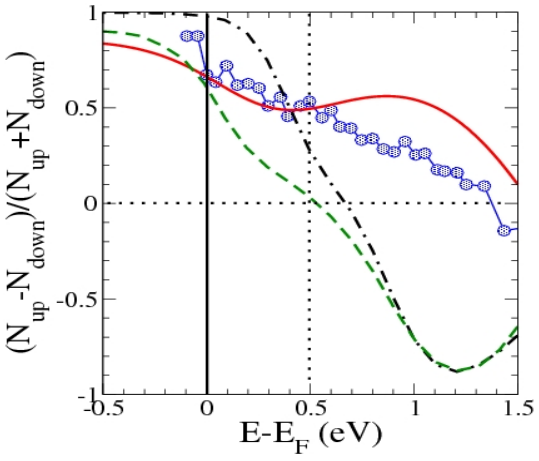


*Fig. 7. Energy dependence of the spin polarization obtained experimentally [5] decorated solid line and different theoretical calculations LDA (dot-dashed), DMFT (dashed), VCA (solid) (Eq. 12) [2]. A broadening of 0.4 eV, corresponding to the experimental resolution, has been added to the theoretical curves.*

## 5. Conclusions

In conclusion, we addressed many-body correlation effects on the electronic structure of $CrO_2$. We derived a minimal three-band Hubbard-Hamiltonian and discussed both the model and realistic parameter for such a Hamiltonian. The many body-problem was solved in the framework of the variational cluster approach, and density of states, spectral function and scaling issues were discussed.

We showed how these many-body effects considerably change the mean-field LSDA+U picture, despite the fact that the interaction is not too strong. More specifically, while in LSDA+U the single occupancy of the Cr $d_{xy}$ orbital is determined by the exchange and crystal field splitting, the competition of the latter with correlation effects, which is taken into account in our variational cluster calculation, induce a ferromagnetic state with an itinerant-type $d_{xy}$ orbital with a large effective mass, rather than localized moments in contrast to previous results [11, 34, 35, 38]. In the minority spin channel, correlations induce non-quasiparticle states which are crucial for the occurrence of spin depolarization in $CrO_2$, as already discussed for other materials [19]. However, a quantitative analysis of depolarisation would require the description of additional effects, such as, e. g., disorder or phonons.

### Acknowledgments

We acknowledge financial support by the Austrian science fund (FWF project P18505-N16) and contract CEEX 20/2005 EXCE-MAG.

### References

[1] M. Imada, A. Fujimori, Y. Tokura, Rev. Mod. Phys. **70**, 1039 (1998).
[2] L. Chioncel, H. Allmaier, A. Yamasaki, M. Daghofer, E. Arrigoni, M. I. Katsnelson, A. I. Lichtenstein, Phys. Rev. B **75**, 140406 (2007).
[3] T. Tsujioka, T. Mizokawa, J. Okamoto, A. Fujimori, M. Nohara, H. Takagi, K. Yamaura, M. Takano, Phys. Rev. B **56**, R15509 (1997).
[4] R. Yamamoto, Y. Moritomo, A. Nakamura, Phys. Rev. B **61**, R5062 (2000).
[5] D. J. Huang, L. H. Tjeng, J. Chen, C. F. Chang, W. P. Wu, S. C. Chung, A. Tanaka, G. Y. Guo, H. – J. Lin, S. G. Shyu, C. C. Wu, C. T. Chen Phys. Rev. B **67**, 214419 (2003).
[6] C. B. Stagarescu, X. Su, D. E. Eastman, K. N. Altmann, F. J. Himpsel, A. Gupta, Phys. Rev. B **61**, R9233 (2000).
[7] K. Suzuki, P. M. Tedrow, Phys. Rev. B 58, 11597 (1998).
[8] E. J. Singley, C. P. Weber, D. N. Basov, A. Barry, J. M. D. Coey, Phys. Rev. B **60**, 4126 (1999).
[9] E. Z. Kurmaev, A. Moewes, S. M. Butorin, M. I. Katsnelson, L. D. Finkelstein, J. Nordgren, P. M. Tedrow, Phys. Rev. B **67**, 155105 (2003).
[10] S. P. Lewis, P. B. Allen, T. Sasaki, Phys. Rev. B **55**, 10253 (1997).
[11] M. A. Korotin, V. I. Anisimov, D. Khomskii, G. A. Sawatzky, Phys. Rev. Lett. **80**, 4305 (1998).
[12] I. I. Mazin, D. J. Singh, C. Ambrosch-Draxl, Phys. Rev. B **59**, 411 (1999).
[13] M. van Veenendaal, A. J. Fedro, Phys. Rev. B **70**, 012412 (2004).

[14] R. A. de Groot, F. M. Mueller, P. G. Engen, K. H. J. Buschow, Phys. Rev. Lett. **50**, 2024 (1983).
[15] K. Schwarz, Journal of Physics F-Metal Physics, **16**, L211 (1986).
[16] R. J. Soulen, J. M. Byers, M. S. Osofsky, B. Nadgorny, T. Ambrose, S. F. Cheng, P. R. Broussard, C. Tanaka, J. Nowak, J. S. Moodera, A. Barry, J. M. D. Coey, Science **282**, 85 (1998).
[17] Y. Ji, G. J. Strijkers, F. Y. Yang, C. L. Chien, J. M. Byers, A. Anguelouch, G. Xiao, A. Gupta, Phys. Rev. Lett. **86**, 5585 (2001).
[18] L. Chioncel, M. I. Katsnelson, R. A. de Groot, A. I. Lichtenstein, Phys. Rev. B. **68**, 144425 (2003).
[19] L. Chioncel, E. Arrigoni, M. I. Katsnelson, A. I. Lichtenstein, Phys. Rev. Lett. **96**, 137203 (2006).
[20] L. Chioncel, Ph. Mavropoulos, M. Lezaic, S. Blugel, E. Arrigoni, M. I. Katsnelson, A. I. Lichtenstein, Phys. Rev. Lett. **96**, 197203 (2006).
[21] L. Chioncel, M. I. Katsnelson, G. A. de Wijs, R. A. de Groot, A. I. Lichtenstein, Phys. Rev. B. **71**, 085111 (2005).
[22] M. Potthoff, M. Aichhorn, C. Dahnken, Phys. Rev. Lett. **91**, 206402 (2003).
[23] M. Potthoff, Eur. Phys. J. B **36**, 335 (2003).
[24] M. Aichhorn, E. Arrigoni, Europhys. Lett. **72**, 117 (2005).
[25] M. Aichhorn, E. Arrigoni, M. Potthoff, W. Hanke, Phys. Rev. B. **74**, 024508 (2006).
[26] S. M. Watts, S. Wirth, S. von Molnar, A. Barry, J. M. D. Coey, Phys. Rev. B. **61**, 9621 (2000).
[27] O. K. Andersen, T. Saha-Dasgupta, Phys. Rev. B. **62**, R16219 (2000).
[28] A. Yamasaki, L. Chioncel, A. I. Lichtenstein, O. K. Andersen, Phys. Rev. B. **74**, 024419 (2006).
[29] A. I. Lichtenstein, M. I. Katsnelson, Phys. Rev. B. **57**, 6884 (1998).
[30] V. I. Anisimov, O. Gunnarsson, Phys. Rev. B. **43**, 7570 (1991).
[31] G. Kotliar, S. Y. Savrasov, K. Haule, V. S. Oudovenko, O. Parcollet, C. A. Marianetti, Rev. Mod. Phys. **78**, 865 (2006).
[32] R. Fresard, G. Kotliar, Phys. Rev. B. 56, 12909 (1997).
[33] E. Pavarini, S. Biermann, A. Poteryaev, A. I. Lichtenstein, A. Georges, O. K. Andersen, Phys. Rev. Lett. **92**, 176403 (2004).
[34] M. S. Laad, L. Craco, E. Muller-Hartman, Phys. Rev. B. **64**, 214421 (2001).
[35]L. Craco, M. S. Laad, E. Muller-Hartmann, Phys. Rev. Lett. **90**, 237203 (2003).
[36] D. M. Edwards, J. A. Hertz Journal of Physics F-Metal Physics **3**, 2191 (1973).
[37] V. Yu. Irkhin, M. I. Katsnelson, J. Phys.: Condens. Matter **2**, 7151 (1990).
[38] A. Toropova, G. Kotliar, S. Y. Savrasov, V. S. Oudovenko, Phys. Rev. B **71**, 172403 (2005).

*Corresponding author: burzo@phys.ubb.cluj.ro